Response to the comments from Anonymous Referee #1

We would like to thank the reviewer for spending their valuable time reviewing our paper, and providing us with invaluable comments.

Here are our responses:

1) Referee Comment: *I found the method description to be technically adequate, but I think this paper would benefit from an expanded discussion of relevance and temporal scale of cryospheric response time: while we might lose half the cooling effects of the cryosphere if Antarctica melts- how realistic is that and over what time scales?*
Even if this is considered outside the scope of this paper, I think it might be useful to relay what the most immediate concern would be and it's associated CrRE.

Our Response: It is true that the component of LCrRE originating from ice sheets and glaciers has a much longer inherent timescale of evolution than that of seasonal snow cover. We agree that it is important to communicate these different timescales, and hence have added statements about this to both the Introduction and Results. Changes in the extent of seasonal snow cover and sea-ice can drive large changes in CrRE on sub-decadal timescales, whereas the areal coverage of ice sheets and glaciers tend to evolve on much longer timescales.

2) Referee Comment: *The mixed use of LCrRE and CrRE acronyms is confusing, I would suggest using one acronym.*

Our Response: Except in the abstract and introduction, we have changed all the acronyms to LCrRE throughout the manuscript. Use of CrRE helps introduce the general concept. Also we did not change the generalized CrRE equation (Eq. 1), which is adapted from Flanner et al., 2011.

3) Referee Comment: *3926, Line 15: You give the timing and peak value for the Northern Hemisphere, but only mention the timing for the Southern Hemisphere- I suggest including both values or neither.*

Our Response: We included both values. It is -9 W/m2 for the Southern Hemisphere.

4) Referee Comment: *3927, Line 4: Consider changing 'cryospheric changes', which is vague, to 'changes in crysospheric extent' or, if you also intend to relay albedo feedbacks ' changes in cryospheric extent and reflectivity'.*

3927, Sentence ending on Line 5: It sounds as if you are saying here that solely cryospheric changes determine the sensitivity of the climate to anthropogenic and external forcings, while you clarify in the next sentence that it is the third most powerful positive feedback, I would suggest altering this sentence.

Our Response: We have changed "cryospheric changes" to "changes in cryospheric extent and reflectivity", as suggested. To soften the second statement that is referred to, we changed "determine" to "partially determine". The subsequent sentence then places the importance of albedo feedback in the broader context of all feedback mechanisms.

5) Referee Comment: *3928, Satellite data description: It wasn't clear to me if the MODIS product used was binary (i.e. snow/no snow), and the snow presence parameter was fractional, or if both were fractional. If the MODIS product was not fractional snow coverage,*

do you think this spatial and temporal scale has any impact over the inclusion of snow in mountainous terrain, which exhibit high variability over relatively short temporal and small spatial scales? Is there reasoning behind using 16 days vs 8 days?

Our Response: The native MODIS snow presence data are binary, but when aggregated over space and time (into a 16-day product at 0.05 degree resolution) the average of this binary quantity becomes fractional. In our analysis, we assumed that any fraction higher than zero indicates the presence of some snow within the gridcell during the 16-day period. We then assumed that any elevation of albedo over the designated snow-free value was caused by snow. In theory, this approach should capture mountainous snow cover, to the extent that it is detected in the native 500m resolution daily MODIS measurements, but considerable variability in mountain snow cover exists on even smaller spatial scales, and cloud masking renders the effective temporal resolution of these data to be longer in practice.

Our definition of LCrRE from mountain *glaciers* is: "permanent glaciated areas between latitudes of 60°S and 60°N". Since the masks used to define these pixels are not time-evolving, the binary snow presence flag does not impact the calculation of this component of the LCrRE. We used the 16 day products because the snow-free albedo dataset was only available at this resolution.

6) Referee Comment: *3929, Line 3: I would suggest instead of saying you 'apply' snow covered information from NISE, you state explicitly state that you fill missing data with snow covered information from NISE, since this is the title of the next section.*

Our Response: That sentence starts with "To derive a spatially and temporally continuous LCrRE record", which we think provides enough indication about how the data were used. Also we have not yet started discussion about filling the pixels at this point in the text, so we did not want to jump ahead with technical details.

7) Referee Comment: *Section 2.2 title: Consider 'Global Albedo Climatology'*

Our Response: We adopted this change.

8) Referee Comment: *Section 3.1: It would help for interpreting results to keep the reportage of them consistent- for example, on page 3933, line 5-6, you report a 0.15% contribution of non-glaciated regions in the southern hemisphere to global LCrRE and then a '3.7 time more' contribution of non-glaciated to glaciated regions in the northern Hemisphere what are these absolute values, or percentage of global LCrRE? And then in line 8 it is stated that LCrRE associated with permanent glacier cover in mountain regions is 'clearly visible'- is there a value associated with this?*

Our Response: The discussion was presented in this way to offer different perspectives to the readers on the contributions from different regions. In response to this comment and comments from Reviewer #2, however, we have added the following two tables to clearly indicate the contributions of the different regions to the global LCrRE. We thank the reviewers for this suggestion.

Table 1b. Percentage contribution of different domains to the global LCrRE using CAM4 kernels

		% Contribution
Northern Hemisphere	Glaciated	8.7 (9.5)
	Non-Glaciated	32.4 (36.6)
Southern Hemisphere	Glaciated	59.7 (54.6)
	Non-Glaciated	0.08 (0.1)
Global	Glaciated	68 (64)
	Non-Glaciated	32 (36)
Global	Global	100 (100)

Table 1c. Percentage contribution of different land masses to the global LCrRE using CAM4 kernels

Land Mass	LCrRE	% Contribution
Antarctica	-1.51 (-1.76)	58.6 (53.6)
Europe+Asia	-0.55 (-0.79)	21.1 (23.94)
North America	-0.34 (-0.49)	13.02 (14.83)
Greenland	-0.19 (-0.25)	7.2 (7.5)
South America	-0.0024 (-0.0043)	0.09 (0.13)
Australia	-2.28E-04 (-4.37E-04)	~0
Africa	-5.59E-05 (-6.2E-05)	~0
Global	-2.58 (-3.28)	100 (100)

For mountain regions, the last paragraph in the same section separately provides all the associated numbers and discussion. We wanted to keep it as a separate point of discussion because it was not resolved well in the older study.

9) Referee Comment: *Flanner et al., 2011 is not in the reference list*

Our Response: Added to the list.

Response to the comments from Anonymous Referee #2

We would like to thank the reviewer for spending their valuable time reviewing our paper, and providing us with invaluable comments.

Here are our responses:

1) Referee Comment: *The paper is titled "cryosphere radiative effect", but it presents only the shortwave effect. There is a longwave effect as well; the presence of the cryosphere reduces both absorbed SW and emitted LW. If Antarctica and Greenland had no ice, those continents would be radiating longwave to space from lower elevation and therefore warmer temperatures. The authors may not want to quantify this LW effect, but they should at least mention it.*

Our Response:

It is true that the LW cryosphere radiative effect may be substantial, and that this study focuses exclusively on the shortwave component of CrRE. We have clarified this through edits to the Abstract and Introduction indicating that the scope of this study is limited to SW effects and that LW effects result from snow-induced changes to surface emissivity and temperature. Quantifying the LW cryosphere radiative effect in a separate study would be a worthy endeavour, but several assumptions and calculations would need to be incorporated, including the surface elevation change (as noted by the reviewer), the change in surface temperature that would result from the lack of insulating snow cover, and the change in surface emissivity.

2) Referee Comment: The second paragraph of Section 3.1 gives some percentage contributions to the global LCrRE. I think Table 1 should be expanded to include these percentages for each of the four regions mentioned (glaciated and non-glaciated NH and SH). I would also like to see a separate table to show contributions to the global LCrRE from each continent (and Greenland). In this second table, one could read (for example) the small total contribution from South America, separated from Antarctica.

Our Response: *We've expanded Table 1 and added these two sub-tables in the paper:*

Table 1b. Percentage contribution of different domains to the global LCrRE using CAM4 kernels

		% Contribution
Northern Hemisphere	Glaciated	8.7 (9.5)
	Non-Glaciated	32.4 (36.6)
Southern Hemisphere	Glaciated	59.7 (54.6)
	Non-Glaciated	0.08 (0.1)
Global	Glaciated	68 (64)
	Non-Glaciated	32 (36)
Global	Global	100 (100)

Table 1c. Percentage contribution of different land masses to the global LCrRE using CAM4 kernels

Land Mass	LCrRE	% Contribution
Antarctica	-1.51 (-1.76)	58.6 (53.6)
Europe+Asia	-0.55 (-0.79)	21.1 (23.94)
North America	-0.34 (-0.49)	13.02 (14.83)
Greenland	-0.19 (-0.25)	7.2 (7.5)
South America	-0.0024 (-0.0043)	0.09 (0.13)
Australia	-2.28E-04 (-4.37E-04)	~0
Africa	-5.59E-05 (-6.2E-05)	~0
Global	-2.58 (-3.28)	100 (100)

3) Referee Comment: *Abstract line 3. Change "Spectrometer" to "Spectroradiometer".*

Our Response: We changed it.

4) Referee Comment: *p 3927 line 18. Change "much of the Antarctic continent" to "West Antarctica".*

Our Response: We changed it.

5) Referee Comment: *p 3928 line 6. Flanner et al 2011 is missing from the reference list.*

Our Response: Added to the list.

6) Referee Comment: *p 3929 line 24. "unfilled pixel". Is this the same as "missing pixel", or does it mean a pixel that is only partly snow-covered?*

Our Response: "Unfilled pixels" are the subset of pixels (only snow-covered) that did not receive defined albedo values in the previous step of the algorithm.

7) Referee Comment: *p 3930 line 14. Removal of the East Antarctic Ice Sheet would indeed expose barren land (albedo 0.26), but removal of the West Antarctic Ice Sheet would instead expose open ocean (albedo 0.07).*

Our Response: This is a very good point, considering the current bed topography. We have decided not to re-do our analysis, however, in light of several other uncertain effects that would occur in the event of total ice sheet ablation. First, isostatic rebound would elevate some of the West Antarctic land mass currently residing below sea level to elevations above sea level. Second, the sea level rise associated with ice ablation would offset some of this effect. Third, new vegetation would encroach onto the continent that would alter the ice-free surface albedo. In light of the uncertainties associated with these additional assumptions, we have chosen not to alter our analysis. Assuming a darker ice-free albedo or West Antarctica would slightly raise (make ~10% more negative) our LCrRE estimates. We have added a brief description of these issues to the manuscript. We also note that the MODIS land mask applied in our study excludes ice shelves.

8) Referee Comment: *Table A1. Why do snow-covered open shrubland (albedo 0.54) and snow-covered grassland (albedo 0.48) have higher albedo than snow-covered barren land (0.37)? Is this because snow depth over barren land is small?*

Our Response: This is a good question, and we can only speculate on the reasons for this. The reviewer's hypothesis of lower snow depth (and consequently increased snow

patchiness) over barren land seems quite plausible, given that barren land is almost always associated with low precipitation and often with high surface wind speeds. Second, a related effect is that barren land may be more susceptible to snow darkening from local wind-blown soil dust. A paper from Wang et al., 2013 (http://onlinelibrary.wiley.com/doi/10.1029/2012JD018291/abstract) provides images and evidence of patchy, dust-darkened snow in regions of China with little or no vegetation, supporting these hypotheses as explanations for lower mean albedos over snow-covered barren land.

9) Referee Comment: *Figure 3. Extend the curves by one additional month, so that the complete seasonal cycle can be seen graphically (i.e. from January to January rather than January to December).*

Our Response: We've extended the plots by one additional month.

The Global Land Cryosphere Radiative Effect during the MODIS era

D. Singh[1], M.G. Flanner[1] and J. Perket[1]

[1] Atmospheric, Oceanic and Space Sciences, Ann Arbor, Michigan, USA

Correspondence to: D. Singh (sdeepak@umich.edu)

Abstract

The shortwave Cryosphere Radiative Effect (CrRE) is the instantaneous influence of snow- and ice-cover on Earth's top of atmosphere (TOA) solar energy budget. Here, we apply measurements from the Moderate Resolution Imaging Spectroradiometer (MODIS), combined with microwave retrievals of snow presence and radiative kernels produced from 4 different models, to derive CrRE over global land during 2001–2013. We estimate global annual mean land CrRE during this period of –2.6 W/m^2, with variations from –2.2 to –3.0 W/m^2 resulting from use of different kernels, and variations of –2.4 to –2.6 W/m^2 resulting from different algorithmic determinations of snow presence and surface albedo. Slightly more than half of the global land CrRE originates from perennial snow on Antarctica, whereas the majority of the northern hemisphere effect originates from seasonal snow. Consequently, the northern hemisphere land CrRE peaks at –6.0 W/m^2 in April, whereas the southern hemisphere effect more closely follows the austral insolation cycle, peaking at -9.0 W/m^2 in December. Mountain glaciers resolved in 0.05 degree MODIS data contribute about –0.037 W/m^2 (1.4%) of the global effect, with the majority (94%) of this contribution originating from the Himalayas. Inter-annual trends in the global annual mean land CrRE are not statistically significant during the MODIS era, but trends are positive (less negative) over large areas of Northern Asia, especially during spring, and slightly negative over Antarctica, possibly due to increased snowfall. During a common overlap period of 2001–2008, our MODIS estimates of the northern hemisphere land CrRE are about 18% smaller (less negative) than previous estimates derived from coarse-resolution AVHRR data, though inter-annual variations are well correlated (r=0.78), indicating that these data are useful in determining longer term trends in land CrRE.

1 Introduction

Snow- and ice-covered surfaces are the most reflective regions on Earth, and their extent can change substantially with small changes in climate. The presence of Earth's cryosphere greatly alters the planet's albedo and ~~cryospheric~~ changes in cryospheric extent and reflectivity therefore partially determine the sensitivity of climate to anthropogenic and external forcings. After water-vapor and cloud feedback, the albedo feedback is the third most powerful positive feedback mechanisms operating within the current climate system (e.g., *Bony et al.,* 2006; *Winton*, 2006; *Randall et al.*, 2007; *Soden et al.*, 2008; *Shell et al.*, 2008; *Flato et al.,* 2013).

Earth's Cryosphere has shown compelling indications of climate change during recent decades, including mass loss from ice sheets and glaciers (e.g., *Rignot et al.*, 2011, *Gardner et al.,* 2013), rapid ablation of autumn Arctic sea-ice (e.g., *Serreze et al.*, 2007; *Stroeve et al*, 2012), and reduced seasonal snow coverage (e.g., *Dery and Brown*, 2007; *Brown and Robinson*, 2011). The Arctic is one of the most sensitive regions on Earth to global climate change *(Manabe et al.,* 1992; *Manabe and Stouffer* 1994; *Miller and Russell* 2000; *Meehl and Washington* 1990). Several recent studies (e.g., *Chapman and Walsh,* 2007, *Monaghan et al.,* 2008, *Steig et al.,* 2009) have shown that climate is also warming over west Antarctica~~much of the Antarctic continent~~, and is related to Pacific Ocean warming (*Ding et al.,* 2011) and circumpolar winds.

The shortwave Cryosphere Radiative Effect (CrRE) is the instantaneous influence of snow- and ice-cover on Earth's top of atmosphere (TOA) solar energy budget (*Flanner et al.*, 2011; *Hudson*, 2011; *Perket et al.,* 2014). CrRE depends not only on snow and sea-ice coverage, but also on local insolation, cloud cover, and properties of the snow, ice and their underlying surface that determine reflectance. These features determine the impacts of cryospheric presence on net TOA solar flux (e.g., *Winton*, 2006; *Qu and Hall,* 2005). Changes in the extent of seasonal snow cover and sea-ice can drive large changes in CrRE on sub-decadal timescales, whereas the areal coverage of ice sheets and glaciers tend to evolve on much longer timescales. The presence of the cryosphere also perturbs Earth's longwave energy budget, e.g., through changes in emissivity and surface temperature resulting from the insulating effect of snow and the change in surface elevation induced by ice sheets. This study, however, concentrating exclusively on the shortwave component of CrRE (hereafter referred to simply as CrRE).

Our work focuses on developing a global, gridded, time-resolved dataset of the land-based CrRE, using modern remote sensing observation of surface albedo and snow presence; combined with radiative kernels that provide TOA radiative impacts. *Flanner et al* (2011) derived a 30-year record of the northern hemisphere CrRE from coarse-resolution determinations of snow cover extent. Here we apply higher-resolution, higher quality remote sensing data from the MODerate-resolution Imaging Spectroradiometer (MODIS) to derive global land-based CrRE over 2001-2013, helping inform on the utility of the longer-term record derived by *Flanner et al* (2011), and broadening the scope of these estimates to include the southern hemisphere. We generate CrRE for both all-sky and clear-sky conditions to help assess the masking effect of clouds and atmospheric aerosols. We provide statistics including global, hemispheric, glaciated and non-glaciated land CrRE averages. We also perform multiple analyses to determine the sensitivity of our estimates to the use of different thresholds for snow cover determinations, different climatologies for missing data, and radiative kernels generated with different distributions of clouds. These sensitivity analyses help us identify the sources of uncertainty that have relatively high impact on CrRE. In this paper, we focus only on land based CrRE, and refer readers to other recent estimates of CrRE from Arctic sea-ice (*Pistone et al.,* 2014; *Cao et al.,* 2015).

2   Methods

2.1   Satellite Dataset Used

MODIS MCD43C3 collection 5 surface albedo data (e.g., *Schaaf et al.,* 2002) and accompanying snow coverage statistic (both provided at spatial resolution 0.05°×0.05°) are the primary input datasets we use to generate land based CrRE (LCrRE) at 16-day resolution. The snow presence parameter (0-100%) is a measure of the fraction of native measurements within each 16-day period and each 0.05° pixel in which the presence of snow was detected. We assume any pixel with snow coverage greater than zero has a surface albedo that was affected by the presence of snow. We apply data with quality flag 4 and better to maximize the spatial and temporal coverage of albedo measurements. Missing data in this collection arise from cloud cover and absence of sunlight at high latitudes during winter. To derive a spatially and temporally continuous LCrRE record, we also apply snow-cover information from the Near-real-time Ice and Snow Extent (NISE) dataset (*Nolin et al.,* 1998), as described in the next subsection. NISE provides daily binary snow-cover at 25 km Equal-Area Scalable Earth Grid (EASE-grid) spatial resolution, projected on a polar stereographic grid. Because it is determined from microwave remote sensing observations, it offers estimates of snow

1 presence under all conditions, including environments with clouds and low illumination.

2 Since these datasets have different spatial resolutions, the NISE dataset has been remapped to

3 the higher resolution MODIS grid prior to analysis.

4 We use global gridded estimates of snow-free albedo derived from MODIS (*Moody et al.*,

5 2008), also provided at 16-day and 0.05 degree resolution, as a baseline for determining the

6 surface albedo contrast induced by snow. These data are climatological 16-day averages

7 derived from 2000-2004 MODIS measurements.

2.2   Global Albedo Climatology for filling missing data

9 A 16-day global surface-albedo climatology with spatial resolution of $0.05°\times0.05°$ is

10 generated to fill any missing MODIS data-points, using the following steps:

11 *Step 1:* For each pixel and each 16-day period of the year, we take the average albedo over all

12 the years (2001-2013) of MODIS data during periods with valid measurements and non-zero

13 snow cover. Since this is a seasonally-varying gridded climatology, it is primarily used to

14 replace albedo of missing MODIS data in situations deemed to be snow-covered in the NISE

15 dataset.

16 *Step 2:* We take the annual mean of the albedo values generated from the previous step for

17 each snow-covered unfilled pixel in step 1. We only apply this average at locations and times

18 when the climatology from step 1 does not provide valid data (e.g., at pixels and 16-day

19 intervals that had substantial cloud cover during each of the 13 years of MODIS

20 observations).

21 *Step 3:* Albedo values generated from the previous two steps are averaged spatially over all

22 pixels within each land classification type defined in the MODIS MCD12C1 product using

23 IGBP (Type 1) land cover classification. This procedure produces an annual-mean snow-

24 covered albedo climatology by land classification (listed in Table A.1), and is used to fill any

25 remaining missing pixels unfilled by steps 1 and 2.

26 MCD12C1 provides the global dominant land cover types at $0.05°\times0.05°$ spatial resolution. It

27 is continuous and therefore completely eliminates the chance of having any missing pixels

28 after applying step 3.

1 Although the snow-free surface albedo dataset is continuous, it is undefined in regions with

2 large solar zenith angle or near-permanent snow cover. To define snow-free albedo in these

3 regions, we apply annual averages of the snow-free albedo values for each pixel (similar to

4 method applied in step 2).

5 The ice-free surface albedo for permanent glaciated areas (e.g. Greenland, Antarctica) is

6 assumed to be 0.26, an average value of snow-free albedo over barren land (*Flanner et al.,*

7 2011). This assumption enables a rough estimate of the TOA impact associated with presence

8 of the full ice sheets. While our estimates of absolute LCrRE in these regions are therefore

9 subject to ambiguities (such as the type of vegetation that would thrive without the ice sheet),

10 seasonal and inter-annual changes in glacier surface albedo, e.g., as caused by altered

11 insolation, melt extent, and snow metamorphic state, drive changes in LCrRE that are

12 unaffected by this assumption, since the ice-free albedo is assumed to be static.

13 Considering the current bed topography removal of the West Antarctic Ice Sheet would

14 expose open-ocean (albedo 0.07). Although, we still use barren land albedo because of

15 several other uncertain effects that would occur in the event of total ice sheet ablation, e.g.,

16 isostatic rebound of land, sea-level rise, encroachment of vegetation over open land. Our

17 objective is to quantify the instantaneous LCrRE and quantifying all the aforementioned

18 uncertainties in this study are beyond the scope of this paper. We also note that the MODIS

19 land mask applied in our study excludes ice shelves.

20 **2.3 Methodology**

21 Our interest lies in the change in solar energy reflected because of snow, and we therefore

22 assume that measured albedo increase in the presence of snow, relative to the snow free state,

23 is caused entirely by snow. *Flanner et al* (2011) employed a definition of CrRE that utilizes

24 snow cover fraction, in order to facilitate the use of snow extent data without coincident

25 albedo measurements from several decades ago. Here we utilize a simpler definition that

26 omits snow cover fraction, since we have direct measurements of surface albedo from

27 MODIS. Using this approach, the mathematical framework to describe CrRE at time t within

28 a region R that is composed of N partially snow- or ice-covered grid-cells i is:

29 $$CrRE(t,R) = \frac{1}{A(R)} \sum_{i=1}^{N} Max\left[\left(\alpha(t,i) - \alpha_{snow-free}(t,i)\right), 0\right] \frac{\partial F}{\partial \alpha}(t,i) A(i) \tag{1}$$

30 where A is area, $\alpha - \alpha_{snow-free}$ is the albedo contrast ($\Delta\alpha$), and $\partial F/\partial\alpha$ is the change in TOA

31 net solar energy flux with changing surface albedo. The 'Max' function is used to avoid any

1   negative albedo contrast values. We determine $\partial F/\partial \alpha$ using radiative kernels that provide

2   the instantaneous effect on TOA energy budget associated with small perturbations in surface

3   albedo (e.g., *Shell et al.,* 2008). This equation is only applied to gridcells where snow

4   presence has been detected, and LCrRE is otherwise assumed to be zero.

5   We created kernel datasets using the general framework of *Perket et al.,* (2014), using the

6   Community Atmosphere Model versions 4 and 5 (CAM4 and CAM5). TOA energy fluxes

7   were calculated with and without surface albedo perturbations every model time-step for one

8   year of simulation, and flux differences were then averaged into monthly resolved kernels.

9   We also apply radiative kernels generated previously with the CAM3 model (*Shell et al.,*

10 2008) and Geophysical Fluid Dynamics Laboratory Atmosphere Model (AM2) (*Soden et al.,*

11 2008).

12 A graphical representation of the basic algorithm used in our analysis is shown in Fig.1,   and

13 can be summarized as follows:

14 a) We first check for the presence of snow in a particular pixel using MODIS data. If snow

15   was present at any time during the 16-day retrieval (snow flag >0) then the difference

16   between actual (16-day) surface albedo and snow-free albedo is taken as the albedo

17   contrast.

18 b) If MODIS data were missing then presence of snow is checked using NISE data. If snow

19   is present during some or all of the 16-day period, then albedo contrast is determined by

20   taking the difference between climatological snow-covered albedo for that gridcell (and

21   time of year, as described in the previous subsection) and snow-free albedo. Since the

22   NISE dataset is continuous and daily-resolved, we are able to determine those situations

23   when a particular pixel was covered with snow for only a portion of the 16-day period of

24   MODIS measurements. In those cases, if a pixel is covered with snow for D days out of

25   16, then the albedo contrast is multiplied with a scaling factor of $D/16$.

26 c) If MODIS determines a pixel is not snow-covered (snow flag = 0) or in the absence of

27   MODIS data if NISE does not indicate any snow ($D = 0$), then albedo contrast and

28   LCrRE are set to zero for that pixel.

29 d) After determining the albedo contrast, this term is multiplied with the various radiative

30   kernels to derive different estimates of all-sky and clear-sky LCrRE. Except as noted in

31   sensitivity studies described later, subsequent LCrRE results are derived from the CAM4

32   radiative kernel, which simulates an intermediate level of cloud masking compared with

33   the other kernels.

3 Results and Discussion

3.1 Spatial and Seasonal Variability of the Mean Climate State

All-sky global annual-mean ~~land-based CrRE~~ (LCrRE) during 2001-2013 calculated using the CAM4 kernel is -2.58 Wm^{-2}, and ranges from -2.16 to -2.96 Wm^{-2} with application of different radiative kernels. Table 1a shows LCrRE averages over different domains and calculated with different radiative kernels. Permanent glaciated regions (e.g., Greenland and Antarctica) contribute about two-thirds of the net global LCrRE, due to their persistently high albedo around the year. For this discussion, land classified as snow or ice in the MODIS MCD12C1 land type dataset (Appendix A) is considered as permanently glaciated.

Due to the size of the Antarctic Ice Sheet, the Southern Hemisphere contributes about 60% of the global LCrRE. On the other hand, non-glaciated regions in Northern Hemisphere contribute about 32% of the global LCrRE. Because the areal extent of seasonal snow has little "memory" beyond a year, non-glaciated component of the LCrRE can respond rapidly to climate change and drive albedo feedback on sub-decadal timescales. Impact of non-glaciated region in Southern Hemisphere is negligible because of less land presence at mid and high latitudes (Fig. 2), contributing only about 0.08~~15~~% of the global LCrRE. In the Northern Hemisphere, non-glaciated regions contribute about 3.7 times more to LCrRE than glaciated areas. LCrRE associated with permanent glacier cover in mountain regions (e.g., the Himalaya) is also clearly visible, even though they are situated at much lower latitudes (Fig. 2). Table 1b and 1c shows percentage contribution of different domains and separate land masses to the global LCrRE respectively.

Clear-sky LCrRE values are expectedly higher than all-sky LCrRE values because of the absence of cloud scattering. Similarly, all-sky LCrRE derived from the CAM5 kernel is higher than that derived from the CAM4 kernel because cloud masking is substantially less in CAM5, due to the prevalence of thinner clouds (*Kay et al.,* 2012, *Perket et al.,* 2014). AM2 and CAM4 values are similar, indicating a similar degree of cloud masking in these two kernels, whereas the CAM3 kernel provides substantially greater attenuation of surface albedo anomalies at the TOA (*Flanner et al.*, 2011). *Cao et al.,* (2015) determined that the CAM3 and AM2 radiative kernels likely mask too much of the Arctic sea-ice radiative effect, but it is unclear if these kernel biases exist over land and have persisted in the more modern CAM4 and CAM5 models.

1   Fig. 3 shows global and hemispheric monthly variations of LCrRE for both all-sky and clear-

2   sky conditions. Seasonal variations are apparent in both hemispheres. LCrRE values peak

3   (become most negative) during April in the Northern Hemisphere, about 2 months before the

4   peak boreal solstice insolation. On the other hand, Southern Hemisphere LCrRE peaks in

5   December, during maximum austral insolation. These differences occur because the Northern

6   Hemisphere LCrRE is dominated by seasonal snow, while Southern Hemisphere LCrRE is

7   dominated by permanent glaciated Antarctica, and thus the seasonal cycle of LCrRE is

8   determined more directly by insolation in the Southern Hemisphere. Spatial distributions of

9   tri-monthly seasonal averages of LCrRE are shown in Fig. 4, indicating the same insolation-

10 modulated tendencies over glaciated terrain described earlier. The timing of peak LCrRE in

11 regions with seasonal snow, however, depends on the timing of melt onset, which almost

12 always precedes the peak insolation period.

13 Peak LCrRE over glaciated regions of the Northern Hemisphere occurs in May, lagging the

14 peak over non-glaciated regions by about one month (Fig. 5). Glaciated LCrRE in the

15 Northern Hemisphere peaks before the summer solstice because Greenland surface albedo

16 decreases between May and the end of June as summer melt commences. This tendency is

17 not apparent over Antarctica because a smaller portion of the Antarctic Ice Sheet experiences

18 surface melt during summer. Also the LCrRE change is more gradual for glaciated than non-

19 glaciated regions during both melting and freezing seasons. As the temperature rises,

20 temporary snow over non-glaciated land ablates relatively quickly. This causes a rapid

21 decrease in surface albedo and hence lowering of the albedo contrast. Similar observations

22 cannot be made for Southern Hemisphere due to negligible LCrRE contribution from non-

23 glaciated region. Global LCrRE values show less seasonal variation than the hemispheric

24 averages because they are basically averages of two hemispheric seasonal cycles that are

25 somewhat out of phase with each other. Nonetheless, global LCrRE does exhibit a minimum

26 during July and August, when there is little seasonal snow cover in the Northern Hemisphere

27 and Antarctica receives little insolation.

28 We observe a contribution of about -0.037 Wm^{-2} (1.43% of the global total) from high

29 mountainous regions (Himalayas, Andes, etc.) towards global LCrRE. The Himalayan region

30 alone contributes about 93.8% of the total mountainous region LCrRE. (Here, we define the

31 high mountainous contribution to LCrRE as that coming from permanent glaciated areas

32 between latitudes of 60°S and 60°N.) The contribution from these high-altitude areas is

33 relatively smaller but consistent throughout the year. Our use of 0.05 degree resolution data

1 allows us to determine LCrRE over many regions with patchy snow extent, though mountain

2 snow cover varies substantially on even smaller spatial scales. Fig. 6 shows LCrRE

3 contribution of the Andes and the Himalayas averaged over the MODIS era.

3.2 Sensitivity Analysis

5 A sensitivity analysis of LCrRE has been done to estimate its dependence on various

6 parameters included in the algorithm (Table 2). In this part of the study, CAM4 kernels are

7 used and other parameters are varied. The first column represents the LCrRE values from the

8 default case using the algorithm discussed in section 2.3 (Fig. 1). The second column lists

9 LCrRE values generated using only the NISE snow flag (i.e., snow presence is determined

10 exclusively with NISE measurements, rather than MODIS). Differences between these

11 estimates are due to the different remote sensing techniques applied to determine snow

12 presence and different spatial and temporal resolutions of the NISE and MODIS datasets.

13 The third and fourth columns are similar to first and second columns, respectively, but apply

14 the land class climatology of albedo contrast instead of spatially- and temporally-varying

15 albedo contrast (section 2.2). The derivation of these land class climatology values is

16 described in step 3 of section 2.2. A list of mean albedo values and standard deviations for

17 the different land classes is provided in Appendix A. In these cases land class climatology

18 albedo values have been used irrespective of data availability in MODIS, in combination with

19 snow presence determined from MODIS+NISE (column 3) and exclusively from NISE

20 (column 4). This sensitivity study is designed to assess the utility of using much simpler

21 estimates of snow-covered albedo than our more involved space- and time-dependent

22 estimates.

23 LCrRE values in the second, third and fourth columns (Table 2) are very similar to each

24 other. In all three cases the estimated LCrRE is lower than the original analysis (column 1).

25 This indicates the dependence of LCrRE on MODIS snow flag and global albedo

26 climatology, and changing either of those drops the LCrRE estimates by about 8% globally.

27 Also when land class climatological albedos are used, LCrRE is very similar for different

28 choice of snow flags. This may be due to the fact that the land class climatology only depends

29 on land class type and does not vary with time.

30 MODIS MCD43C3 albedo data are accompanied by quality flags, indicating the fraction of

31 input measurements to each 16-day data point that were made under cloud-free conditions

32 with sufficiently small solar zenith angle (e.g., *Schaaf et al,* 2002). Table 3 shows a

comparative study of LCrRE determined without quality flag filtering (i.e., quality flag 4 and better), and determined using only quality flag 2 or better albedo data. Quality flag 2 is mixed, with 75% or less of the underlying data derived from inverting reflectance for the BRDF retrievals, and 25% or less of the underlying data filled. Using better albedo data (lower quality flag) does not make a significant difference in our determination of global LCrRE. This indicates that the fill values applied in the MCD43C3 retrieval algorithm are similar to our developed climatology (section 2.2).

3.3   Inter-annual trends

Annual global LCrRE averages do not show significant inter-annual trends during the MODIS era (Fig. 7), perhaps partially due to the relatively short duration of this period. Slopes for global, northern hemisphere and southern hemisphere LCrRE are -2×10^{-3} $Wm^{-2}yr^{-1}$, -1.3×10^{-3} $Wm^{-2}yr^{-1}$ and 7.3×10^{-4} $Wm^{-2}yr^{-1}$, respectively. These trends are not significant at the 95% confidence level.

To better understand the LCrRE trend, pixel-by-pixel trend maps have been generated using the Mann-Kendall regression technique with 95% significance level (Fig. 8). A strong positive trend (indicating less negative LCrRE) is observed over some regions of the Northern Hemisphere, especially over Northern Asia during the spring season (Fig. 8b). Positive trends over seasonally snow covered areas are most likely due to a decrease in snow coverage (e.g., *Qu and Hall,* 2007; *Vaughan et al.,* 2013), and the trend in LCrRE that we find over Northern Asia is consistent with studies showing recent declines in snow cover over this region (e.g., *Dery and Brown*, 2007; *Brown and Robinson*, 2011). Possible reasons for the positive trends seen over Greenland include: 1) increased snow metamorphism and black carbon deposition (e.g., *Box et al,* 2012; *Keegan et al., 2014*), 2) transport and deposition of dust and other light-absorbing impurities over the ice-sheets due to increased dust source areas associated with increased snow-free area (*Dumont et al.,* 2014), and 3) MODIS sensor degradation on the Terra satellite during recent years (*Sun et al.,* 2014*; Lyapustin et al.,* 2014), which would indicate a spurious decline in albedo.

We also observe slightly negative LCrRE trends over Antarctica, which may be due to increases in snowfall that have decreased the duration that surface snow has to "age", thereby increasing surface albedo (*Picard et al.,* 2012). Interestingly, LCrRE has also become more negative over some regions of Central Asia, presumably due to increased temporal coverage of snow.

3.4 Comparison with previous study

The current study and that of *Flanner et al.,* (2011) have a common overlap period of 2001-2008. To compare the derivations of LCrRE between these two studies, we re-derived Northern Hemisphere LCrRE during 2001-2008 using the CAM3 radiative kernel and an assumption of ice-free albedo over Greenland of 0.316, as in *Flanner et al.* (2011). For this overlap period, and using these assumptions, the current study gives a LCrRE value of about -1.41 Wm^{-2} over the northern hemisphere as compared to -1.72 Wm^{-2} from *Flanner et al.,* (2011), who determined snow presence during 1979-2008 from coarse-resolution AVHRR data (e.g., *Robinson et al,* 2000). (The 1979-2008 mean northern hemisphere LCrRE found by *Flanner et al,* (2011) was -2.0 W/m^2, indicating less boreal cryospheric influence during 2001-2008 compared with 1979-2001). To understand this difference, an LCrRE difference map between the current study and *Flanner et al.,* (2011) has been generated (Fig. 9). This difference was taken between annual mean LCrRE values over the common overlap period. We find that the use of coarse-resolution snow cover data (*Flanner et al,* 2011) likely leads to overestimation of LCrRE along the continental edges and in mountainous regions like the Himalayas. Some of the differences along the continental edges (especially of Greenland), depicted in Fig. 9 at 1 degree resolution, are likely due to poor resolution of land cover fraction in the AVHRR snow cover data used by *Flanner et al* (2011), and possibly also the influence of land-fast sea-ice. Snow in mountainous regions is difficult to resolve in any model because of irregular topography, and is uncertain in both datasets. The annual mean LCrRE time-series (Fig. 10) of both datasets show similar patterns and exhibit a correlation coefficient of 0.78, lending confidence in the application of longer-term AVHRR data to derive estimates of large-scale LCrRE trends. We expect that the current analysis will be useful in determining correction algorithms for biases in the Himalayas and along the coastal margins of Greenland that may result from use of coarse-resolution AVHRR data.

4 Conclusions

We have estimated a global land-based CrRE (LCrRE) of about -2.6 Wm^{-2} during 2001-2013, with about 59% of the effect originating from Antarctica. For a particular region, LCrRE can vary significantly (e.g., from 0 to -250 Wm^{-2} over Antarctica; Fig. 5) depending on the season. Due to a large contribution from seasonal snow, northern hemisphere LCrRE peaks during April, whereas southern hemisphere LCrRE peaks during the December solstice. About 78% of Northern Hemisphere LCrRE originates from seasonal or non-glaciated snow while about 99.9% of Southern Hemisphere LCrRE comes from glaciated areas.

Mountainous region provide a small (-0.037 Wm^{-2}) yet consistent contribution towards LCrRE throughout the year. Higher resolution data has improved the LCrRE estimates relative to previous studies by better resolving the snow impact in mountainous regions and in coastal areas, leading to a 18% smaller estimate of northern hemisphere LCrRE during 2001-2008 in this study than in *Flanner et al.* (2011). Inter-annual variations between these two studies are well correlated (*r*=0.78), indicating that these data are useful in determining longer term trends in ~~land~~ LCrRE.

Snow cover, however, is patchy on substantially smaller spatial scales than the 0.05 degree resolution analysis applied here. No significant trend over time has been observed in global annual LCrRE values between 2001 and 2013, though significant reductions in cryospheric influence are evident over large areas of northern Eurasia, especially during spring. Slightly negative LCrRE trends (indicating increased albedo) are evident over Antarctica, possibly due to increased snowfall frequency. LCrRE primarily depends on albedo contrast induced by snow and the propagation of surface albedo anomalies to top-of-atmosphere energy fluxes. A slight variation in either of the two can cause a major impact on LCrRE estimates. Sensitivity analysis shows a secondary dependency of LCrRE on MODIS snow flag and global climatology derived using MODIS surface albedo product, and changing either of those drops the LCrRE estimates by about 8% globally. Using different MODIS data quality flags (Q2 & Q4) does not have a significant effect on our LCrRE estimates. Using different radiative kernels can cause a variation of about 3-16% in global LCrRE as compared to LCrRE with the CAM4 kernel, depending on the atmospheric attenuation present in each particular model due to cloud cover and aerosols.

Appendix A: Snow-covered albedo climatology by land classification

Definitions for different land classes used in the MODIS MCD12C1 product are provided by the International Geosphere-Biosphere Programme (IGBP). Table A.1 provide mean (μ) and standard deviation (σ) of surface albedo for each land class type using section 2.2 algorithm.

Acknowledgements

References

Bony, S., Colman, R., Kattsov, V.M., Allan, R.P., Bretherton, C.S., Dufresne, J-L., Hall, A., Hallegatte, S., Holland, M. M., Ingram, W., Randall, D.A., Soden, B.J., Tselioudis, G., and Webb, M. J.: How Well Do We Understand and Evaluate Climate Change Feedback Processes?. J. Climate, 19, 3445–3482. doi: 10.1175/JCLI3819.1, 2006.

Brown, R. D., and Robinson, D. A.: Northern hemisphere spring snow cover variability and change over 1922-2010 including an assessment of uncertainty, The Cryosphere, 5 (1), 219-229, doi:10.5194/tc-5-219-2011, 2011.

Cao, Y., Liang, S., Chen, X., and He, T.: Assessment of Sea Ice Albedo Radiative Forcing and Feedback over the Northern Hemisphere from 1982 to 2009 Using Satellite and Reanalysis Data. J. Clim., 28, 1248–1259. doi: 10.1175/JCLI-D-14-00389.1, 2015.

Chapman, W. L., and Walsh, J. E.: A synthesis of Antarctic temperatures. J. Clim. 20 (16), 4096-4117, doi:10.1175/JCLI4236.1, 2007.

Dery, S. J., and Brown, R. D.: Recent Northern Hemisphere snow cover extent trends and implications for the snow-albedo-feedback, Geophys. Res. Lett., 34, L22504, doi:10.1029/2007GL031474, 2007.

Ding, Q., Steig, E., Battisi, D., and Kuttel, M.: Winter warming in West Antarctica caused by central tropical Pacific warming. Nature Geoscience 4, 398-403, doi:10.1038/ngeo1129, 2011.

Dumont, M., Brun, E., Picard, G., Michou, M., Libois, Q., Petit, J. R., Geyer, M., Morin, S., & Josse, B.: Contribution of light-absorbing impurities in snow to Greenland's darkening since 2009. Nature Geoscience, 7, 509–512, doi:10.1038/ngeo2180, 2014.

Flanner, M. G., Shell, K. M., Barlage, M.,Perovich, D. K., and Tschudi, M. A., Radiative forcing and albedo feedback from the Northern Hemisphere cryosphere between 1979 and 2008, Nature Geoscience., 4(3), 151–155, doi:10.1038/ngeo1062, 2011.

Flato, G., J. Marotzke, B. Abiodun, P. Braconnot, S.C. Chou, W. Collins, P. Cox, F. Driouech, S. Emori, V. Eyring, C. Forest, P. Gleckler, E. Guilyardi, C. Jakob, V. Kattsov, C. Reason and M. Rummukainen, 2013: Evaluation of Climate Models. In: *Climate Change 2013: The Physical Science Basis. Contribution of Working Group I to the Fifth Assessment*

Report of the Intergovernmental Panel on Climate Change [Stocker, T.F., D. Qin, G.-K. Plattner, M. Tignor, S.K. Allen, J. Boschung, A. Nauels, Y. Xia, V. Bex and P.M. Midgley (eds.)]. Cambridge University Press, Cambridge, United Kingdom and New York, NY, USA, 741–866, doi:10.1017/CBO9781107415324.020.

Gardner, A. S., Moholdt, G., Cogley, J. G., Wouters, B., Arendt, A. A., Wahr, J., Berthier, E., Hock, R., Pfeffer, W. T., Kaser, G., Ligtenberg, S. R. M., Bolch, T., Sharp, M. J., Hagen, J. O., van den Broeke, M. R., and Paul, F.: A reconciled estimate of glacier contributions to sea level rise: 2003 to 2009. Science, 340, 852-857, 2013.

Kay, J. E., Holland, M.M., Bitz, C. M., Blanchard-Wrigglesworth, E., Gettelman, A., Conley, A., and Bailey, D.: The influence of local feedbacks and northward heat transport on the equilibrium Arctic climate response to increased greenhouse gas forcing, J. Clim., 25(16), 5433–5450, doi:10.1175/JCLI-D-11-00622.1, 2012.

Keegan, K. M., Albert, M. R., McConnell, J. R., & Baker, I.: Climate change and forest fires synergistically drive widespread melt events of the Greenland Ice Sheet. Proceedings of the National Academy of Sciences,111(22), 7964-7967, 2014.

Lyapustin, A., Wang, Y., Xiong, X., Meister, G., Platnick, S., Levy, R., Franz, B., Korkin, S., Hilker, T., Tucker, J., Hall, F., Sellers, P., Wu, A., and Angal, A.: Scientific impact of MODIS C5 calibration degradation and C6+ improvements, Atmos. Meas. Tech., 7, 4353-4365, doi:10.5194/amt-7-4353-2014, 2014.

Manabe, S., and Stouffer, R. J.: Multiple-century response of a coupled ocean– atmosphere model to an increase of atmospheric carbon dioxide. J. Clim., 7, 5–23, 1994.

Manabe, S., Spelman, M. J., and Stouffer, R.J.: Transient response of a coupled ocean–atmosphere model to gradual changes of atmospheric CO2. Part II: Seasonal response. J. Clim., 5, 105–126, 1992.

Meehl, G. A., and Washington, W. M.: CO_2 climate sensitivity and snow-sea-ice parameterization in an atmospheric GCM coupled to a mixed-layer ocean model. Climate Change, 16**,** 283–306, 1990.

Miller, J. R., and Russell, G. L.: Projected impact of climatic change on the freshwater and salt budgets of the Arctic Ocean by a GCM. Geophys. Res. Lett., 27, 1183–1186, 2000.

Monaghan, A. J., Bromwich, D. H., Chapman, W., and Comiso, J.: Recent variability and trends of Antarctic near-surface temperature. Journal of Geophysical Research, 113, D04105, doi: 10.1029/2007JD009094, 2008.

Moody, E. G., King, M. D., Schaaf, C. B., and Platnick, S.: MODIS-derived spatially complete surface albedo products: Spatial and temporal pixel distribution and zonal averages, J. Appl. Meteor., 47 (11), 2879-2894, doi:10.1175/2008JAMC1795.1, 2008.

Nolin, A., Armstrong, R. L., and Maslanik, J.: Near-Real-Time SSM/I-SSMIS EASE-Grid Daily Global Ice Concentration and Snow Extent. Version 4 (2001-2013). Boulder, Colorado USA: NASA DAAC at the National Snow and Ice Data Center, 1998.

Perket, J., Flanner, M. G., and Kay, J. E.: Diagnosing shortwave cryosphere radiative effect and its 21st century evolution in CESM, J. Geophys. Res. Atmos., 119, 1356–1362, doi:10.1002/2013JD021139, 2014.

Picard, G., Domine, F., Krinner, G., Arnaud, L. and Lefebvre, E., Inhibition of the positive snow-albedo feedback by precipitation in interior Antarctica, Nature Climate Change, vol. 2, 795 -798, 2012.

Pistone, K., Eisenman, I., and Ramanathan, V.: Observational determination of albedo decrease caused by vanishing Arctic sea ice. Proc. Natl. Acad. Sci. USA, 111, 3322–3326, doi:10.1073/pnas.1318201111, 2014.

Qu, X. & Hall, A.: Surface contribution to planetary albedo variability in cryosphere regions. J. Clim. 18, 5239-5252, 2005.

Qu, X., Hall, A.: What controls the strength of snow-albedo feedback?. J. Clim. 20: 3971-3981, 2007.

Robinson, D. A., and Frei, A.: Seasonal variability of northern hemisphere snow extent using visible satellite data, Professional Geographer, 51, 307-314, 2000.

Schaaf, C. B., Gao, F., Strahler, A. H., Lucht, W., Li, X. W., Tsang, T., Strugnell, N. C., Zhang, X. Y., Jin, Y. F., Muller, J. P., Lewis, P., Barnsley, M., Hobson, P., Disney, M., Roberts, G., Dunderdale, M., Doll, C., D'entremont, R. P., Hu, B. X., Liang, S. L., Privette, J.

L., And Roy, D.: First operational BRDF, albedo nadir reflectance products from MODIS. Remote Sensing of Environment, 83, 135–148, 2002.

Serreze, M. C., Holland, M. M., and Stroeve, J.: Perspectives on the arctic's shrinking sea-ice cover, Science, 315, 1533-1536, doi:10.1126/science.1139426, 2007.

Shell, K. M., Kiehl, J. T. & Shields, C. A.: Using the radiative kernel technique to calculate climate feedbacks in NCAR's community atmospheric model. J. Clim. 21, 2269-2282, 2008.

Soden, B. J., Held, I. M., Colman, R., Shell, K. M., Kiehl, J. T., and Shields, C. A.: Quantifying climate feedbacks using radiative kernels, J. Clim., 21(14), 3504–3520, doi:10.1175/2007JCLI2110.1, 2008.

Steig, E., Schneider, D. P., Rutherford, S. D., Mann, M., Comiso, J. C., and Shindell, D. T.: Warming of the Antarctic ice-sheet surface since the 1957 International Geophysical Year. Nature 457, 459-462, doi: 10.1038/nature07669, 2009.

Stroeve, J., Hamilton, L., Bitz, C. M., and Blanchard-Wrigglesworth, E.: Predicting September Sea Ice: Ensemble Skill of the SEARCH Sea Ice Outlook 2008–2013. Geophysical Research Letters, 41, 2411–2418, doi: 10.1002/2014GL059388, 2014.

Sun, J., Xiong, X., Angal, A., Chen, H., Wu, A., and Geng, X.: Time-dependent response versus scan angle for MODIS reflective solar bands. Geoscience and Remote Sensing, IEEE Transactions on 52.6: 3159-3174, 2014.

Vaughan, D.G., J.C. Comiso, I. Allison, J. Carrasco, G. Kaser, R. Kwok, P. Mote, T. Murray, F. Paul, J. Ren, E. Rignot, O. Solomina, K. Steffen and T. Zhang, 2013: Observations: Cryosphere. In: *Climate Change 2013: The Physical Science Basis. Contribution of Working Group I to the Fifth Assessment Report of the Intergovernmental Panel on Climate Change* [Stocker, T.F., D. Qin, G.-K. Plattner, M. Tignor, S.K. Allen, J. Boschung, A. Nauels, Y. Xia, V. Bex and P.M. Midgley (eds.)]. Cambridge University Press, Cambridge, United Kingdom and New York, NY, USA, 317–382, doi:10.1017/CBO9781107415324.012, 2013.

Winton, M.: Surface albedo feedback estimates for the AR4 climate models. J. Clim. 19, 359-365, 2006.

Table 1a. All-sky (Clear-Sky) Cryosphere Radiative Effect averaged over different domains and derived with various radiative kernels (Wm^{-2})

		CAM4 kernel	CAM5 kernel	CAM3 kernel	AM2 kernel
Northern Hemisphere	Glaciated	-0.45 (-0.62)	-0.56 (-0.63)	-0.36 (-0.61)	-0.45 (-0.60)
	Non-Glaciated	-1.67 (-2.4)	-1.95 (-2.48)	-1.16 (-2.42)	-1.40 (-2.24)
Southern Hemisphere	Glaciated	-3.08 (-3.58)	-3.41 (-3.61)	-2.79 (-3.58)	-3.16 (-3.59)
	Non-Glaciated	-0.004 (-0.007)	-0.005 (-0.008)	-0.003 (-0.007)	-0.004 (-0.007)
Global	Glaciated	-1.77 (-2.1)	-1.99 (-2.12)	-1.58 (-2.09)	-1.81 (-2.09)
	Non-Glaciated	-0.84 (-1.2)	-0.98 (-1.25)	-0.58 (-1.21)	-0.70 (-1.12)
Global	Global	-2.58 (-3.28)	-2.96 (-3.37)	-2.16 (-3.31)	-2.51 (-3.22)

Table 1b. Percentage contribution of different domains to the global LCrRE using CAM4 kernels

		% Contribution
Northern Hemisphere	Glaciated	8.7 (9.5)
	Non-Glaciated	32.4 (36.6)
Southern Hemisphere	Glaciated	59.7 (54.6)
	Non-Glaciated	0.08 (0.1)
Global	Glaciated	68 (64)
	Non-Glaciated	32 (36)
Global	Global	100 (100)

Table 1c. Percentage contribution of different land masses to the global LCrRE using CAM4 kernels

Land Mass	**LCrRE**	**% Contribution**
Antarctica	-1.51 (-1.76)	58.6 (53.6)
Europe+Asia	-0.55 (-0.79)	21.1 (23.94)
North America	-0.34 (-0.49)	13.02 (14.83)
Greenland	-0.19 (-0.25)	7.2 (7.5)
South America	-0.0024 (-0.0043)	0.09 (0.13)
Australia	-2.28E-04 (-4.37E-04)	~0
Africa	-5.59E-05 (-6.2E-05)	~0
Global	-2.58 (-3.28)	100 (100)

Table 2. All-sky (Clear-Sky) CrRE (Wm^{-2}) derived with different algorithms. All cases apply the CAM4 radiative kernels.

		Both flags with original climatology	Only NISE flag with original climatology	Both flags with land class climatology	Only NISE flag with land class climatology
Northern Hemisphere	Glaciated	-0.45 (-0.62)	-0.37 (-0.51)	-0.39 (-0.54)	-0.38 (-0.51)
	Non-Glaciated	-1.67 (-2.4)	-1.4 (-2.0)	-1.41 (-2.05)	-1.47 (-2.1)
Southern Hemisphere	Glaciated	-3.08 (-3.58)	-3.03 (-3.51)	-2.91 (-3.38)	-2.91 (-3.38)
	Non-Glaciated	-0.004 (-0.007)	-0.004 (-0.006)	-0.005 (-0.008)	-0.008 (-0.012)
Global	Glaciated	-1.77 (-2.1)	-1.7 (-2.0)	-1.65 (-1.96)	-1.65 (-1.95)
	Non-Glaciated	-0.84 (-1.2)	-0.7 (-1.0)	-0.71 (-1.03)	-0.74 (-1.05)
Global	Global	-2.58 (-3.28)	-2.4 (-3.01)	-2.36 (-2.99)	-2.38 (-3.0)

Table 3. All-sky (Clear-Sky) CrRE (Wm^{-2}) with different quality flag filters, derived using CAM4 kernels in all cases.

|		Quality flag 4 or better	Quality flag 2 or better
Northern Hemisphere	Glaciated	-0.45 (-0.62)	-0.43 (-0.59)
	Non-Glaciated	-1.67 (-2.4)	-1.6 (-2.29)
Southern Hemisphere	Glaciated	-3.08 (-3.58)	-3.07 (-3.57)
	Non-Glaciated	-0.004 (-0.007)	-0.004 (-0.006)
Global	Glaciated	-1.77 (-2.1)	-1.75 (-2.08)
	Non-Glaciated	-0.84 (-1.2)	-0.8 (-1.15)
Global	Global	-2.58 (-3.28)	-2.55 (-3.23)

Table A.1. Mean (μ) and standard deviation (σ) of snow-covered surface albedo for different land class types. The averaging filter used to determine snow presence was based on both MODIS and NISE datasets of snow, and thus these averages are specific to the current study. MODIS provides surface albedo only over land, so albedo for water cannot be determined.

Land Class Type	Mean (μ)	Std Dev (σ)
Water	N/A	N/A
Evergreen Needleleaf forest	0.30	0.008
Evergreen Broadleaf forest	0.21	0.005
Deciduous Needleleaf forest	0.33	0.024
Deciduous Broadleaf forest	0.33	0.018
Mixed forest	0.29	0.013
Closed shrublands	0.42	0.023
Open shrublands	0.54	0.046
Woody savannas	0.40	0.025
Savannas	0.46	0.031
Grasslands	0.48	0.038
Permanent wetlands	0.41	0.027
Croplands	0.49	0.036
Urban and built-up	0.37	0.019
Cropland/Natural vegetation mosaic	0.41	0.026
Snow and ice	0.72	0.033
Barren or sparsely vegetated	0.37	0.023
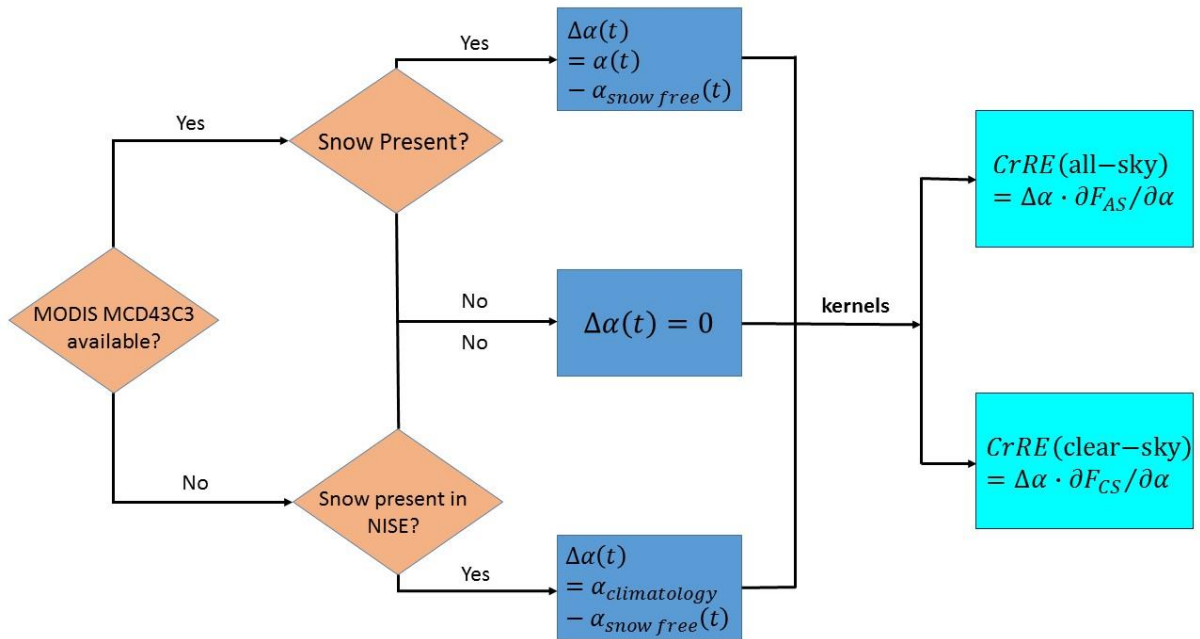
1

2   Figure 1: Algorithm for calculating CrRE.

3
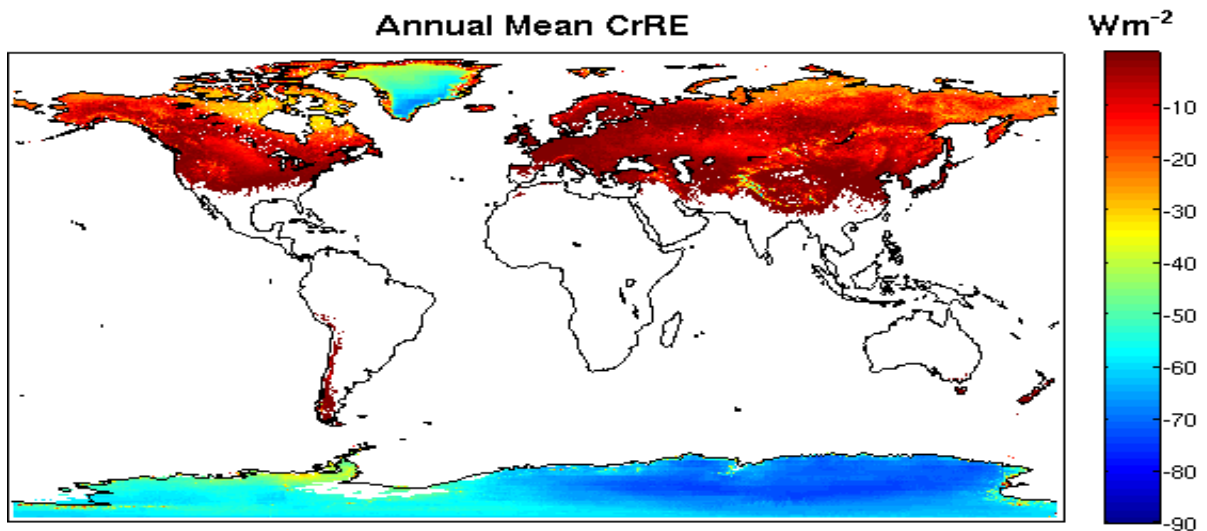
4
5

6   Figure 2. Map showing annual-mean all-sky land CrRE, averaged over 2001-2013, derived
7   with the CAM4 kernel.

1
2
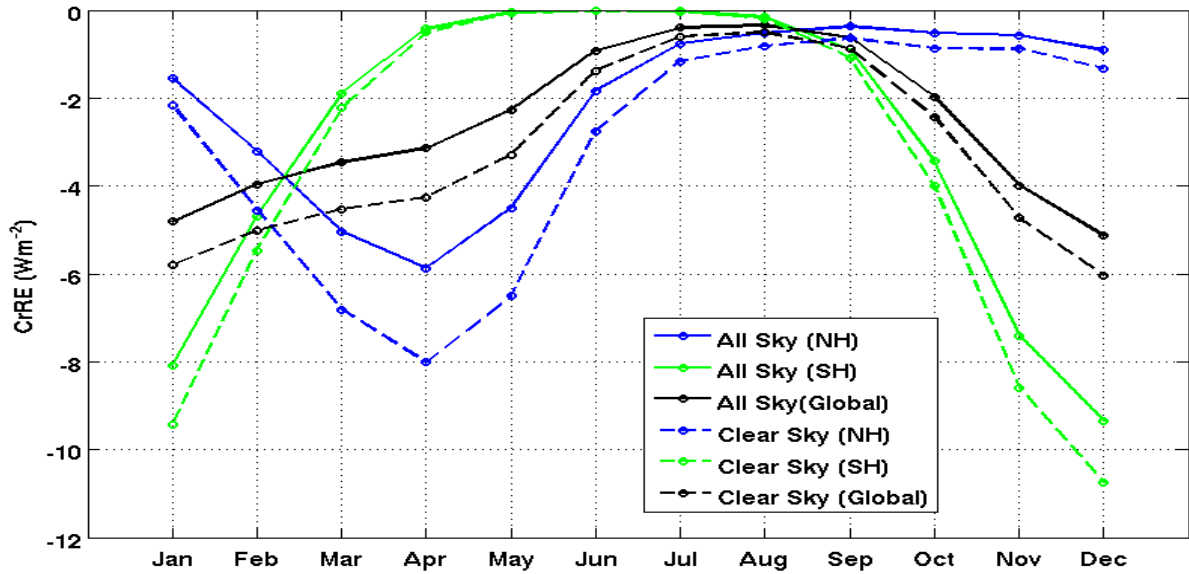
Figure 3. Annual cycle of hemispheric and global ~~land~~ LCrRE for both all-sky and clear-sky
conditions, derived from the CAM4 radiative kernels.

5
6
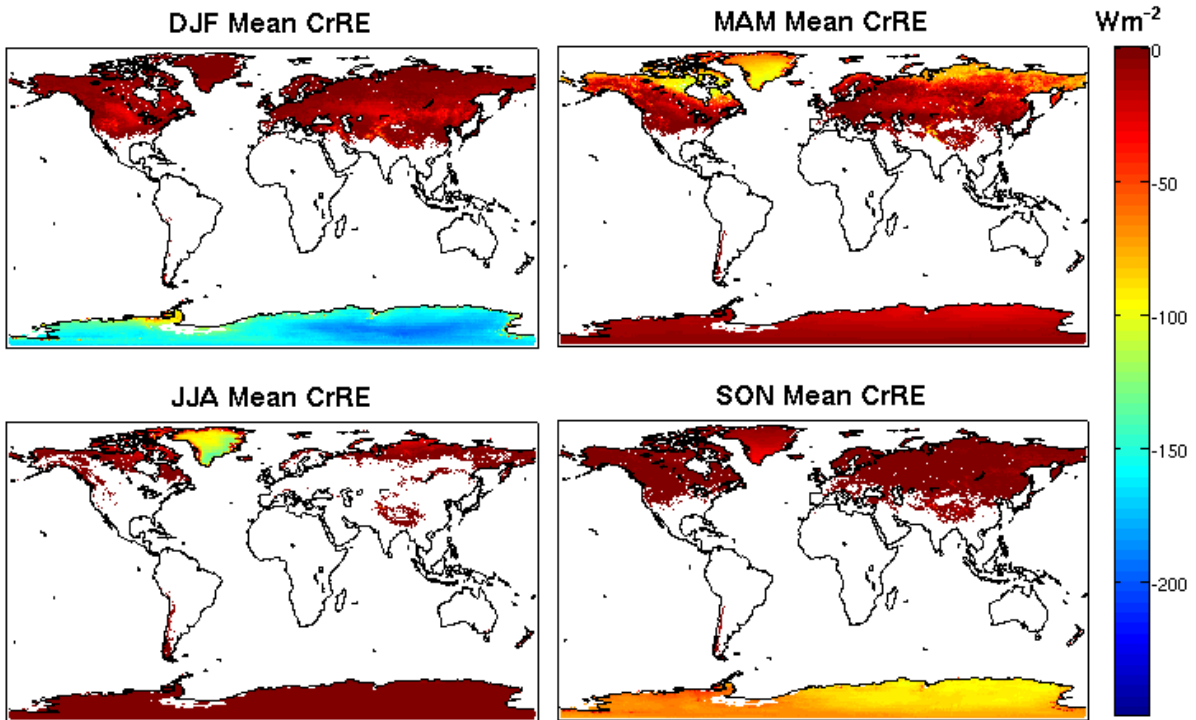
7
8

Figure 4. Tri-monthly seasonally averaged ~~land~~ LCrRE derived with the CAM4 all-sky
kernel. (DJF – December, January, February; MAM – March, April, May; JJA – June, July,
August; SON – September, October, November).
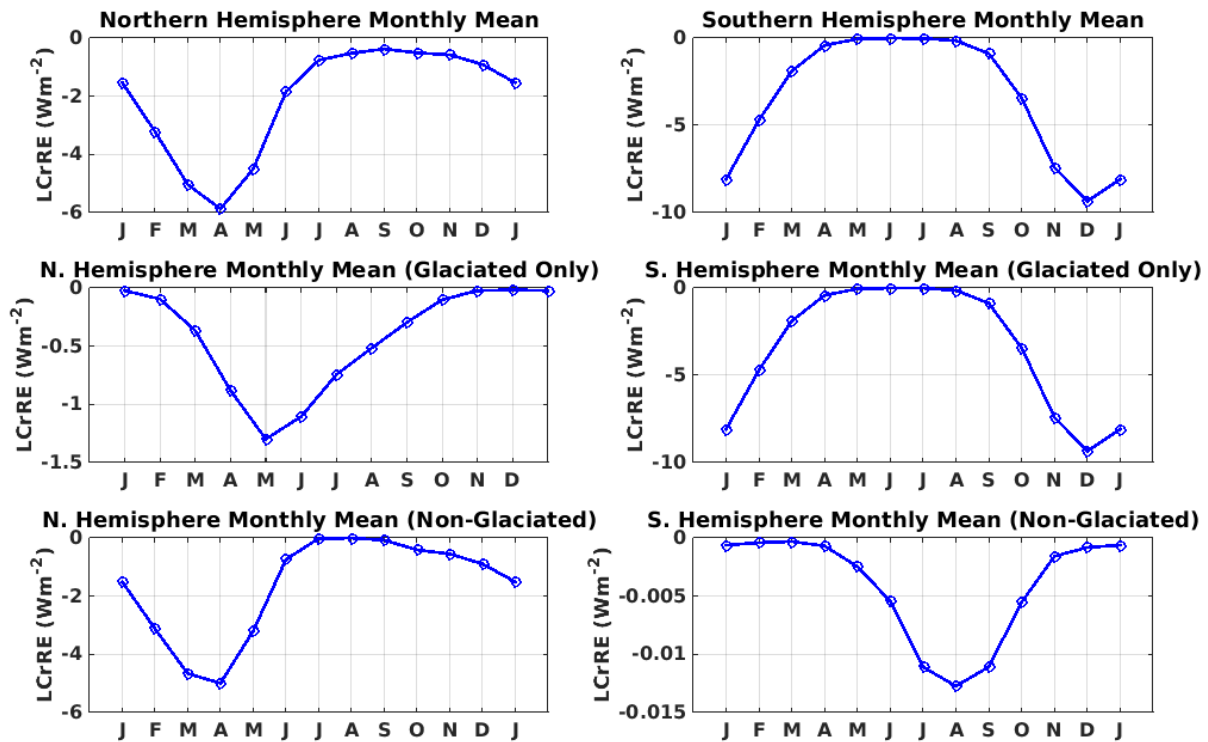
Figure 5. All-sky LCrRE averaged over the Northern (left) and Southern (right) Hemisphere, shown as contributions from all land within the hemisphere (top), permanently glaciated areas only (middle), and non-glaciated areas only (bottom). Data were derived with the CAM4 radiative kernel.
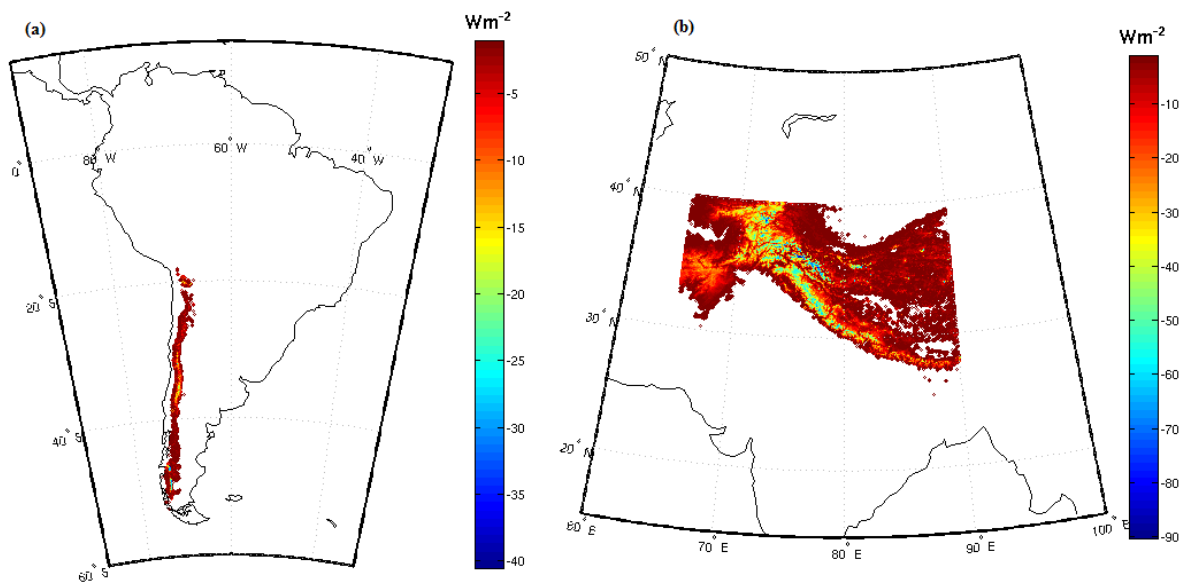
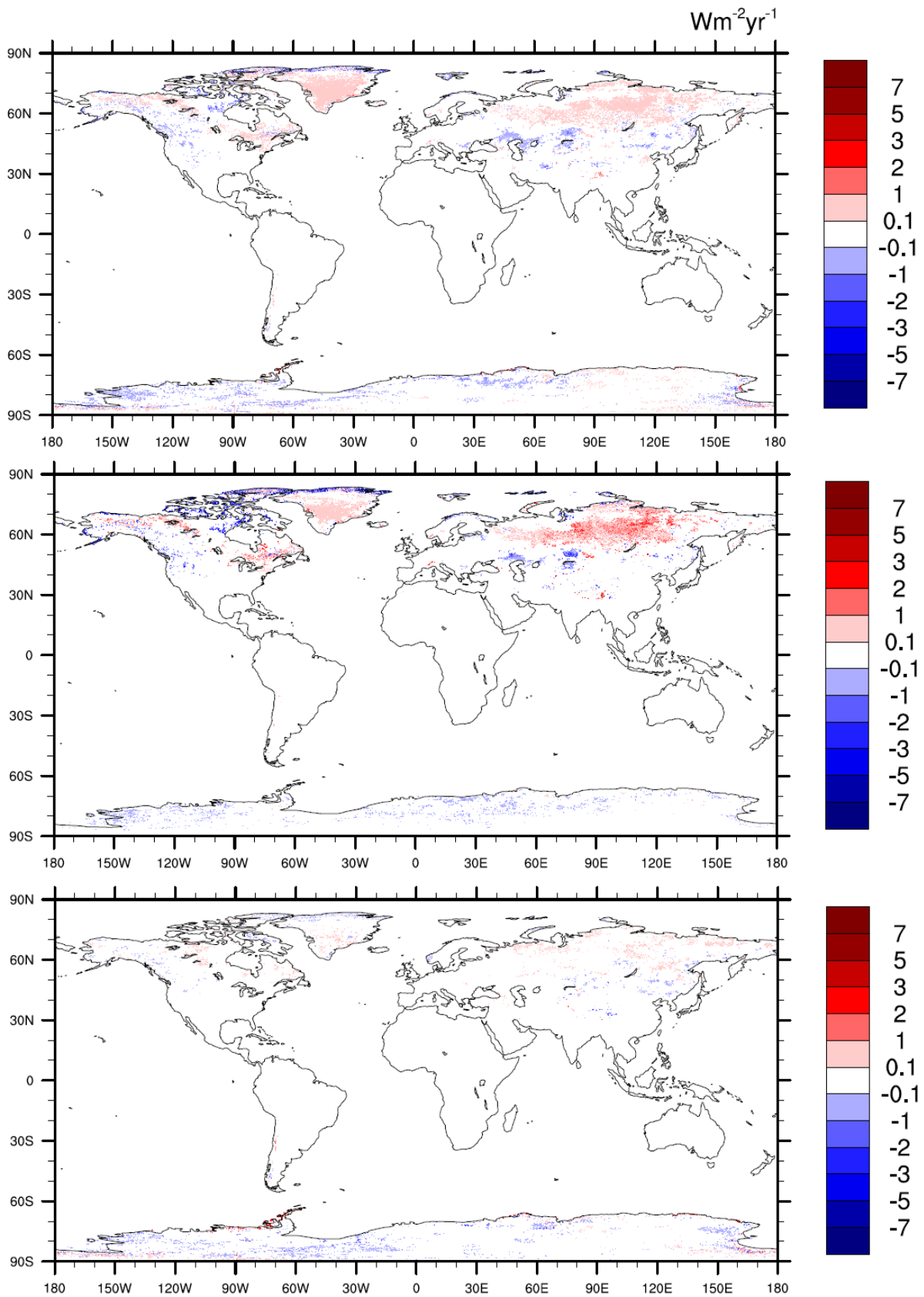Figure 6. Maps showing all-sky LCrRE, averaged over 2001-2013 over (a) Andes and (b) Himalayan mountain ranges.

1
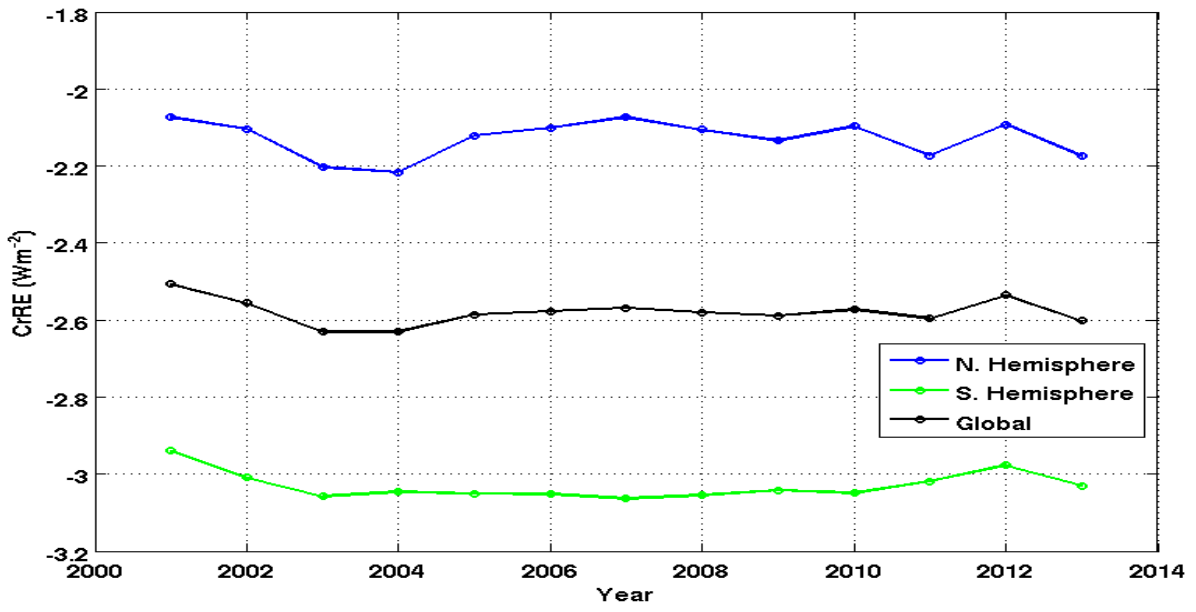
2
3

4 Figure 7. Annual mean land LCrRE time series during 2001-2013 for the globe and each
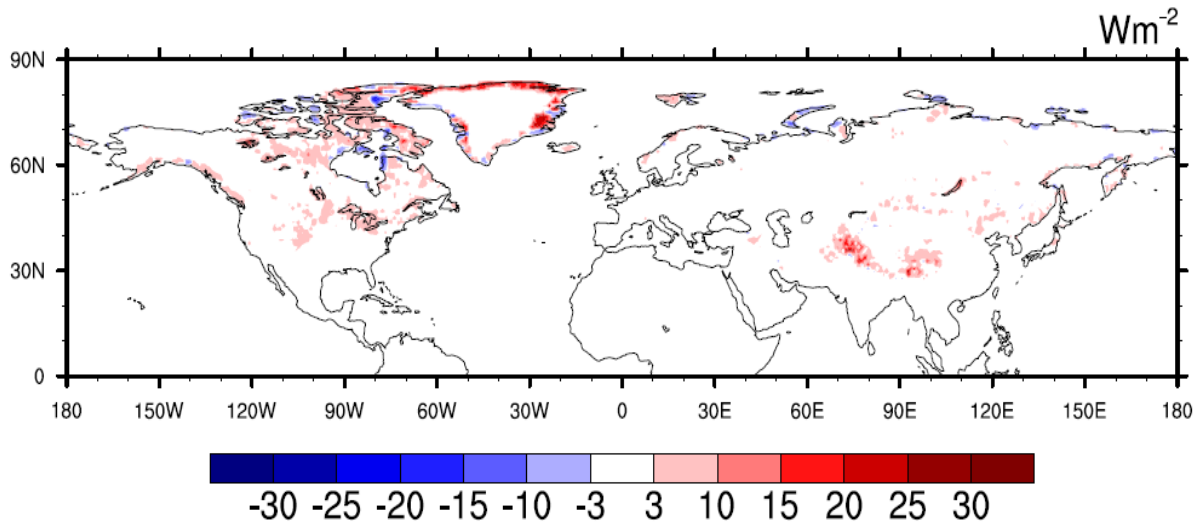5 hemisphere.

1

2

Figure 8. LCrRE trend maps for annual (Top), MAM (Middle) and SON (Bottom) seasons
(MAM – March, April, May; SON – September, October, November). Trends were derived

1   using Mann-Kendall regression technique. Only regions with significant trends (p=0.05) are
2   shown in the map.

3
4

5   Figure 9**.** Difference of 2001-2008 mean LCrRE between the current study and *Flanner et al.,*
6   (2011) using CAM3 kernels. Areas of red indicate a stronger (more negative) LCrRE
7   determined by *Flanner et al* (2011) than determined here.

8

9
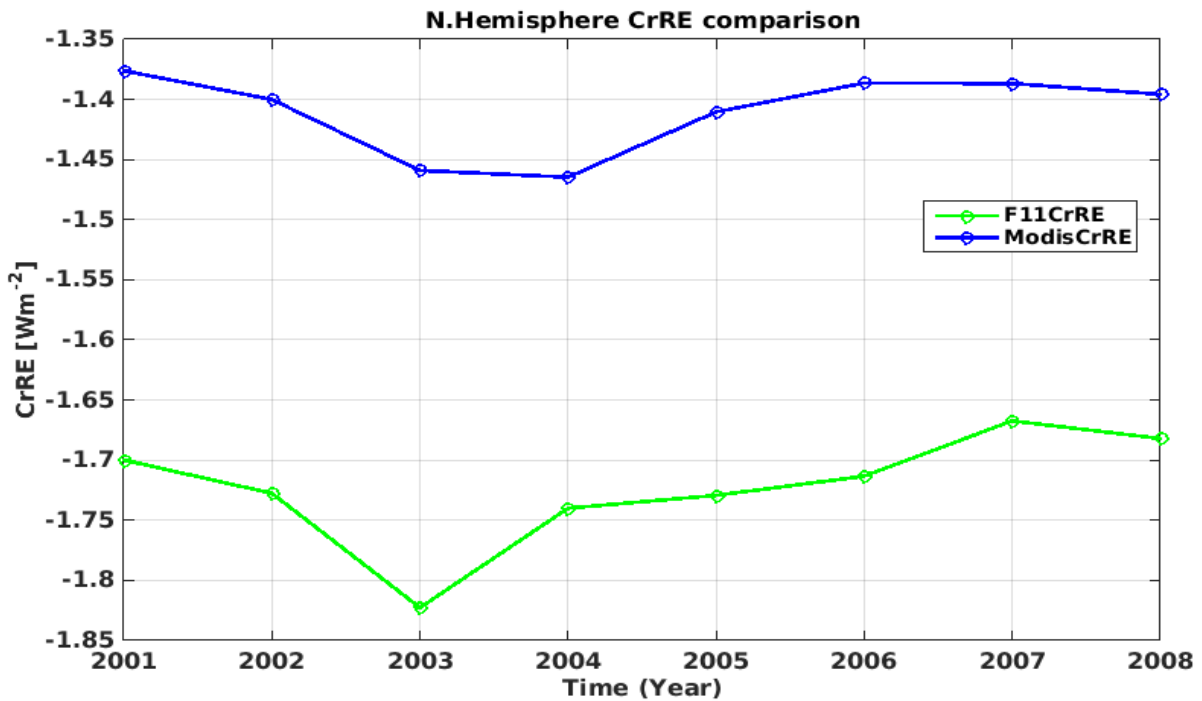
10
11

12   Figure 10. Annual mean Northern Hemisphere LCrRE timseries derived for the current study
13   (ModisCrRE) and by *Flanner et al.,* (2011) (F11CrRE) using CAM3 kernels.